Dyakonov-Perel spin relaxation in InSb/$Al_xIn_{1-x}Sb$ quantum wells

Jun Li,[1] Kai Chang,[1,*] and F. M. Peeters[2]
[1]*SKLSM, Institute of Semiconductors, Chinese Academy of Sciences, P.O. Box 912, Beijing 100083, China*
[2]*Department of Physics, University of Antwerp, Groenenborgerlaan 171, B-2020 Antwerpen, Belgium*
(Received 26 June 2009; revised manuscript received 21 September 2009; published 22 October 2009)

We investigate theoretically the Dyakonov-Perel spin relaxation time by solving the eight-band Kane model and Poisson equation self-consistently. Our results show distinct behavior with the single-band model due to the anomalous spin-orbit interactions in narrow band-gap semiconductors, and agree well with the experiment values reported in recent experiment [K. L. Litvinenko *et al.*, New J. Phys. **8**, 49 (2006)]. We find a strong resonant enhancement of the spin relaxation time appears for spin align along $[1\bar{1}0]$ at a certain electron density at 4 K. This resonant peak is smeared out with increasing the temperature.

DOI: 10.1103/PhysRevB.80.153307 PACS number(s): 72.25.Rb, 71.28.+d, 71.70.Ej

Spin relaxation time (SRT) is very important for the coherent manipulation of electron spin and applications in spintronics devices. There are four different spin relaxation mechanisms,[1] i.e., the D'yakonov-Perel' (DP),[2] Elliott-Yafet (EY),[3] Bir-Aronov-Pikus,[4] and hyperfine interaction[5] mechanism. Among them, the DP mechanism is found to be the dominating spin relaxation mechanism in zinc blende semiconductor structures over a wide range of temperature.[6] According to the DP theory, the electrons lose their initial spin orientation due to a momentum-dependent effective magnetic field that changes its orientation frequently which is caused by random impurity scattering. Therefore the momentum-dependent effective magnetic field is the key factor to determine the spin relaxation time, and it is induced by two types of spin-orbit interactions (SOIs) in structures without inversion symmetry, i.e., the Rashba SOI (RSOI) arising from structure inversion asymmetry and the Dresselhaus SOI (DSOI) caused by bulk inversion asymmetry. In conventional semiconductor quantum structures, the DP theory based on the single-band model with linear momentum-dependent SOIs have been demonstrated to agree well with the experiments, e.g., GaAs/AlGaAs quantum well (QW),[7] and InGaAs/InP QW.[8] Recently, the spin relaxation time in narrow band-gap semiconductor InSb/AlInSb QW also attracted much interest,[9–11] because of its unusual properties for spintronics devices, e.g., small electron effective mass, strong spin-orbit coupling, and large effective Landé g factor. However, the SOIs in narrow band-gap semiconductor is quite different from the single-band model with linear momentum-dependent SOIs. For example, the Rashba spin-splitting exhibits a nonlinear behavior while the kinetic energy of the electron is comparable to the band gap.[12] Therefore, a detailed theoretical investigation beyond the single band model for the DP spin relaxation time is necessary in the case of narrow band-gap InSb/AlInSb QW for the potential spintronics device and basic physics.

In this Brief Report, we investigate theoretically the DP spin relaxation time and its dependencies on the temperature, electron density, and the thickness of the InSb/AlInSb QW. The effective magnetic field and the spin relaxation time is calculated based on the self-consistent solution of the eight-band Kane Hamiltonian and the Poisson equation. We find that the effective magnetic field obtained from the eight-band model deviates strongly from that obtained by the single-band model with the momentum-linear SOI. We show that the eight-band model results are in good agreement with experiment values without introducing any fitting parameter. We find a strong anisotropic SRT: a strong resonant peak of SRT for spins aligned along the $[1\bar{1}0]$ direction can be seen by tuning the electron density since electron at $T=4$ K. But this peak is gradually smeared out with increasing temperature. Our results could be helpful to observe new physical phenomenon, e.g., the intrinsic spin Hall effect and persistent spin helix[13] in such narrow band-gap InSb/AlInSb QWs.

We consider an asymmetric n-doped InSb/AlInSb QW grown along the [001] crystallographic direction [see Fig. 1(a)]. The n-doping layer is assumed to be located 20 nm on the left side of the InSb well and with an exponentially decaying profile. We extend the previous theory (see Refs. 15 and 16) to the framework of the eight-band model by changing all operators in two-band model to the eight-band model,[17,18] the DP spin relaxation time τ_α ($\alpha=+,-,z$, representing the spin relaxation time for the spin of the injected electrons oriented along [110], $[1\bar{1}0]$, and [001], respectively) can be written as

$$\frac{1}{\tau_\alpha} = 4\frac{\tau_{tr}}{\hbar^2}\frac{\xi_\alpha^\nu}{\zeta^0}\frac{\zeta^\nu}{\zeta^{\nu+1}}, \tag{1}$$

with

$$\xi_\alpha^\nu = \sum_s \int_0^\infty d\boldsymbol{k}\Gamma_{s,\alpha}(\boldsymbol{k})[E_s^r(\boldsymbol{k})]^\nu \Delta F_{s,+}(E_F,\boldsymbol{k}), \tag{2}$$

and

$$\zeta^\nu = \sum_s \int_0^\infty d\boldsymbol{k}[E_s^r(\boldsymbol{k})]^\nu \Delta F_{s,+}(E_F,\boldsymbol{k}). \tag{3}$$

Here, $E_s^r(\boldsymbol{k}) \equiv E_s(\boldsymbol{k}) - E_s(0)$ is the kinetic energy of an electron in the s-th sub-band, $\Delta F_{s,+}(E_F,\boldsymbol{k}) \equiv F_{s,+}(E_F,\boldsymbol{k}) - F_{s,-}(E_F,\boldsymbol{k})$ is the Fermi distribution difference between the spin-up and spin-down sub-band, τ_{tr} is the transport relaxation time and $\Gamma_{s,\alpha}(\boldsymbol{k})$ ($\alpha=+,-,z$) is the spin relaxation rates

$$\Gamma_{s,+}(\boldsymbol{k}) = \Lambda_{xx} + \Lambda_{yy} - \Lambda_{xy} - \Lambda_{yx}, \tag{4}$$

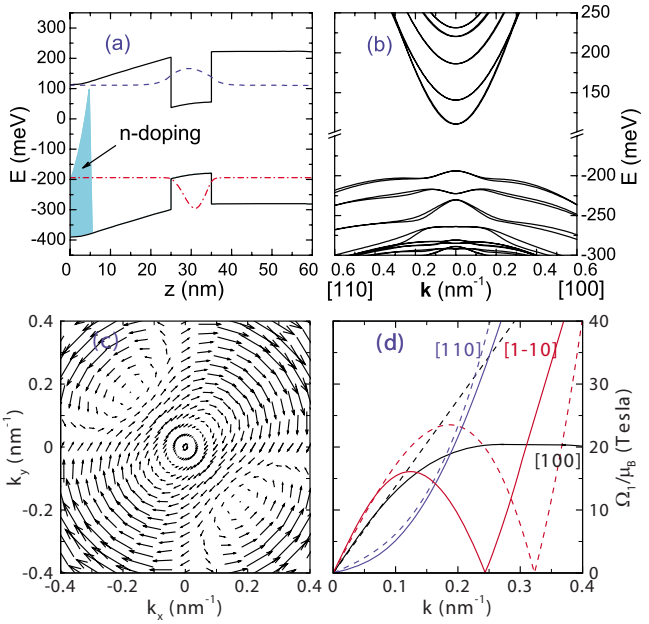

FIG. 1. (Color online) (a) The calculated band alignment and electron (hole) probability distribution. The shading area describes the doping profile. The sheet carrier density is $n_e=5.2\times10^{11}$ cm^{-2}. (b) The self-consistently calculated energy dispersions of electron. (c) The vectors of effective magnetic field $\mathbf{\Omega}_1(\boldsymbol{k})$ on k_x-k_y plane (d) The magnitude of the effective magnetic field $\Omega_1(\boldsymbol{k})$ for $\boldsymbol{k}$ along [100](black solid line) [110] (blue dashed line) and $[1\bar{1}0]$ (red dash-dotted line) of an asymmetrically n-doped $InSb/Al_{0.15}In_{0.85}Sb$ QW at $T=4$ K.

$$\Gamma_{s,-}(\boldsymbol{k}) = \Lambda_{xx} + \Lambda_{yy} + \Lambda_{xy} + \Lambda_{yx}, \tag{5}$$

$$\Gamma_{s,z}(\boldsymbol{k}) = \Lambda_{zz}, \tag{6}$$

with

$$\Lambda_{ij} = 4\sum_{n=-\infty}^{\infty}\left[\sum_{l}\Omega_{s,l}^{-n}\Omega_{s,l}^{s,n}\delta_{ij} - \Omega_{s,j}^{-n}\Omega_{s,i}^{n}\right]\eta^{n,\nu} \tag{7}$$

$$\eta^{n,\nu} = \int_0^{2\pi}\frac{1-\cos\theta}{\sin^{2\nu}(\theta/2)}\Big/\int_0^{2\pi}\frac{1-\cos(n\theta)}{\sin^{2\nu}(\theta/2)}, \tag{8}$$

$$\Omega_{s,i}^{n}(k) = \int_0^{2\pi}\frac{d\varphi_k}{2\pi}\Omega_{s,i}(\boldsymbol{k})e^{-in\varphi_k}. \tag{9}$$

$\mathbf{\Omega}_{s,i}(\boldsymbol{k})$ $(i=x,y)$ is the components of the in-plane effective magnetic field of the s-th sub-band. $\mathbf{\Omega}_{s,i}(\boldsymbol{k})$ can be obtained by ascribing the spin-splitting induced by space inversion asymmetry to the Zeeman splitting caused by the effective magnetic field. Therefore, by using the eight-band Zeeman term[16] $H_z=\mu_B\boldsymbol{B}\cdot\Sigma$, $\mathbf{\Omega}_{s,i}(\boldsymbol{k})$ can be written as

$$\Omega_{s,i}(\boldsymbol{k}) \equiv \mu_B B_i = \frac{S_{s,i}(\boldsymbol{k})\Delta E_s(\boldsymbol{k})}{2\sqrt{S_{s,x}(\boldsymbol{k})^2 + S_{s,y}(\boldsymbol{k})^2}}, \tag{10}$$

$$S_{s.i}(\boldsymbol{k}) = \langle\psi_{s,+}(\boldsymbol{k})|\Sigma_i|\psi_{s,+}(\boldsymbol{k})\rangle - \langle\psi_{s,-}(\boldsymbol{k})|\Sigma_i|\psi_{s,-}(\boldsymbol{k})\rangle. \tag{11}$$

$\Sigma_i(i=x,y)$ is the components of the eight-band effective spin matrices which can be found in Ref. 18 and 19. $\Delta E_s(\boldsymbol{k}) \equiv E_{s,+}(\boldsymbol{k}) - E_{s,-}(\boldsymbol{k})$ is the spin-splitting of the s-th sub-band. The eigenenergy $E_{s,\pm}(\boldsymbol{k})$ and eigenstates $|\psi_{s,+}(\boldsymbol{k})\rangle$ can be numerically obtained by solving the eight-band Kane Hamiltonian and the Poisson equation self-consistently.[18] Through this approach, the nonparabolic effect and the anomalous behavior of SOIs in narrow band-gap semiconductors can be taken into account. In Eqs. (1)–(8), ν is a constant characterizing the relation of momentum scattering time on the electron kinetic energy $(\tau_p(\boldsymbol{k}) \propto [E_s^r(\boldsymbol{k})]^\nu)$. For acoustic phonon and screened ionized impurities scattering (type I), $\nu=0$, for polar optical phonon scattering (type II), $\nu=1$, for weekly screened ionized impurities (type III), $\nu=2$.[16]

In Figs. 1(a) and 1(b) we show the calculated potential profile, the electron probability and the energy dispersion of a 10-nm $InSb/Al_{0.15}In_{0.85}Sb$ QW at $T=4$ K including the effect of built-in electric field caused by the charge redistribution. All the Kane parameters of the materials used in our calculation are taken from Ref. 20, and the ratio of the conduction band offset and the conduction band offset is taken as 62%:38%.[21] The bulk inversion asymmetry of zinc blende crystal is introduced by the B parameter in the eight-band Kane Hamiltonian,[22] which is taken to be $B=31.4$ eV·Å.[11] Besides, we should notice that the temperature dependence of the band gap (Varshini relation)[14] is more pronounced in a narrow band gap semiconductor than that in a wide band gap semiconductor, for instance, the bulk band gap of InSb, of which the bulk band gap is 0.235 eV at 4 K, and 0.174 eV at 300 K, i.e., up to a 26% variation in the band gap with increasing temperature. Because the SOI and spin-splitting is intimately related to the conduction-valence band coupling, the decreasing of band gap could lead to an enhancement of the SOI and results in the increasing in electron sub-band spin-splitting and the effective magnetic field (about 11%).

Figure 1(c) shows the effective magnetic field as a function of the in-plane momentum. The effective magnetic field of a (001)-grown InSb/AlInSb QW always lie in the QW plane. Due to the interplay of RSOI and DSOI, the effective magnetic field exhibits a C_{2v} symmetry. Notice that the effective magnetic field is enhanced or weakened when $\boldsymbol{k}$ along the [110] or $[1\bar{1}0]$ directions. Figure 1(d) shows the self consistent eight-band modeling for the magnitude of the effective magnetic field for $\boldsymbol{k}$ along [100], [110], $[1\bar{1}0]$ (see the solid curves). Along $[1\bar{1}0]$ crystallographic direction, the effective magnetic field pointing along $[\bar{1}\bar{1}0]$ vanishes at a certain Fermi wave vector $\boldsymbol{k}$, which makes the spin lifetime τ_- become very long. In Fig. 1(d) we compare these results with those from the single-band model with $\boldsymbol{k}$-linear SOI. One can see clearly that the deviation of effective magnetic field is very large (up to 42%) at $\boldsymbol{k}=0.2$ nm^{-1}([100]). This deviation comes from the weakening of the interband coupling as the electron kinetic energy becomes comparable to the band gap. Therefore the single-band model may not be good enough to describe the strong SOIs in such narrow band-gap QWs.

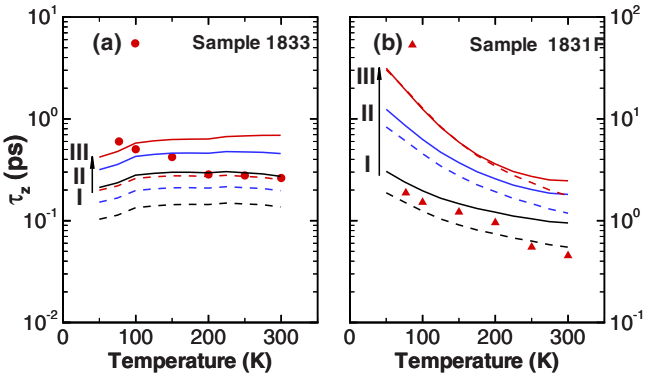

FIG. 2. (Color online) Calculated spin relaxation time τ_z versus temperature compare to the experimental results reported in Ref. 9. (a) Sample 1833 (asymmetrically n-doped 20-nm $InSb/Al_{0.15}In_{0.85}Sb$ QW) (b) Sample 1831F (uniformly n-doped 20-nm $InSb/Al_{0.15}In_{0.85}Sb$ QW). The black, blue, and red lines represent the eight-band numerical results for type I (ν=0), type II (ν=1), and type III (ν=2) momentum scattering mechanism. The dashed lines with the same colors represent the results from the single-band model with linear SOI.

In Fig. 2, we compare the numerical results of SRT τ_z with the experimental measurement reported in Ref. 9. The transport momentum relaxation time τ_{tr} used in our calculation are obtained from the measured Hall mobility [by $\tau_{tr}=m^*\mu_{\mathrm{Hall}}/(e r_{\mathrm{Hall}})$].[16] The electron density is assumed to increase linearly from 3.6×10^{11} cm^{-2} to 5.3×10^{11} cm^{-2} for sample 1833 and from 5.7×10^{11} cm^{-2} to 7.3×10^{11} cm^{-2} for sample 1831F when temperature increase from 77 to 300 K. Considering different momentum relaxation mechanisms, our eight-band numerical results agree quite well with the experiment values without having to introduce any fitting parameter. From panel (a), we can see the weekly screened impurity scattering (ν=2) and polar phonon scattering (ν=1) dominate at $T<150$ K and the ionized impurity scattering dominates at $T>150$ K. Noticed that in heavily doped semiconductor samples, the dominant momentum scattering mechanisms varied through neutral (weekly screened) impurities scattering, acoustic and polar phonon scattering, and ionized impurity scattering with increasing temperature,[23] therefore our results are reasonable and also consistent with the previous work.[16,24] One can see that, due to the overestimate of SOI strength by the linear SOI model, the single-band model will underestimate the SRT compared to the eight-band model and doesn't agree with the measured SRT. For the uniformly doped sample 1831F, our calculated DP SRT is larger than the measured value. The discrepancy between the calculated DP SRT from the eight-band model with measured value is reasonable because the SRT induced by the EY mechanism could be comparable to the DP SRT.[9] The calculated SRT from the single-band model in this symmetric doped sample is similar with that from the eight-band model. This is because the cubic DSOI term (the RSOI is absent due to symmetric doping) in this sample may play a dominant role.

In Fig. 3, we calculate the spin relaxation times τ_z, τ_+, and τ_- as a function of electron density n_e in a 10-nm n-doped $InSb/Al_{0.15}In_{0.85}Sb$ QW for different temperatures. As shown

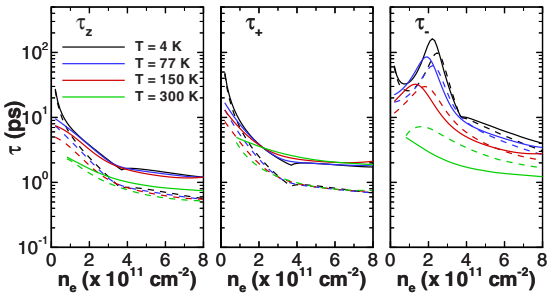

FIG. 3. (Color online) Spin relaxation times τ_z, τ_+, and τ_- as a function of electron density n_e in a 10-nm asymmetric n-doped $InSb/Al_{0.15}In_{0.85}Sb$ QW for different temperature. The dashed lines with the same colors represent the results of single-band model with linear SOI.

in the figure, the SRTs τ_z, τ_+ decrease with increasing electron density due to the enhancement of SOIs with increasing the Fermi wave vector. When temperature increases, the τ_z and τ_- are suppressed strongly, but τ_+ is not very sensitive to temperature. The giant spin relaxation anisotropy[11,15,16] is also demonstrated in InSb/AlInSb QW: the SRT of the $[1\bar{1}0]$-oriented spins shows a resonant peak at a certain electron density at low temperature. However, the resonant peak is very sensitive to temperature. As temperature increases from 4 to 300 K, the peak is gradually smeared out, which is due to the blurring of the Fermi surface with increasing temperature. The dashed lines show the results of the single-band model. Consistent with the former discussion, the results of the single-band model is smaller than that of the eight-band model but at small n_e.

In Fig. 4, we exhibit the SRTs τ_z, τ_+, and τ_- as a function of electron density in a 10-nm n-doped $InSb/Al_{0.15}In_{0.85}Sb$ QW for different thicknesses of InSb well. The SRTs increase with increasing thickness of the InSb well when the electron density n_e is small, but has an opposite trend when the electron density n_e are larger than a certain value. The resonant peak value of τ_- becomes larger and the corresponding n_e becomes smaller with increasing thickness of the QW. The results of the single-band model is smaller than that of the eight-band model except at small n_e.

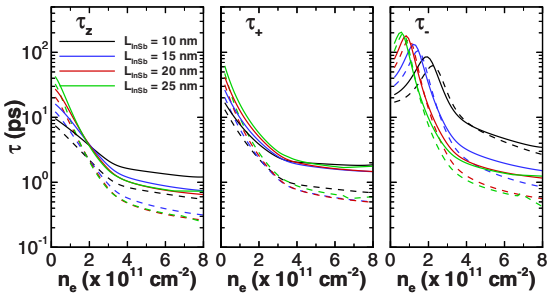

FIG. 4. (Color online) Spin relaxation times τ_z, τ_+, and τ_- as a function of carrier density in asymmetric n-doped $InSb/Al_{0.15}In_{0.85}Sb$ QWs. The dashed lines with the same colors represent the results of the single-band model with linear SOI.

In summary, we investigated theoretically the SRT in InSb/AlInSb QW beyond the single-band model. Our results are obtained within the eight-band model and agree very well with the measured SRTs, while the SRT obtained from the single-band model with linear momentum-dependent SOIs deviates strongly from that of the eight-band model due to the strong interband coupling in narrow band gap QWs. We also demonstrate that the SRT along $[1\bar{1}0]$ direction shows a resonant peak at a certain electron density, i.e., very long SRT. The resonant peak will be smeared out with increasing temperature.

This work is supported by the NSFC under Grants No. 60525405 and No. 10874175, and the bilateral program between China and Belgium, and the Belgian Science Policy (IAP).

*kchang@red.semi.ac.cn

[1] I. Žutić, J. Fabian, and S. Das Sarma, Rev. Mod. Phys. **76**, 323 (2004).
[2] M. I. D'yakonov and V. I. Perel', Fiz. Tverd. Tela (Leningrad) **13**, 3581 (1971) [Sov. Phys. Solid State **13**, 3023 (1972)].
[3] R. J. Elliott, Phys. Rev. **96**, 266 (1954).
[4] G. L. Bir, A. G. Aronov, and G. E. Pikus, Zh. Eksp. Teor. Fiz. **69**, 1382 (1975) [Sov. Phys. JETP **42**, 705 (1975)].
[5] M. I. D'yakonov and V. I. Perel', Pis'ma Zh. Eksp. Teor. Fiz. **13**, 206 (1971) [JETP Lett. **13**, 144 (1971)].
[6] G. E. Pikus and A. N. Titkov, in *Optical Orientation*, edited by F. Meier and B. P. Zakharchenya (Elsevier, Amsterdam, 1984).
[7] Y. Ohno, R. Terauchi, T. Adachi, F. Matsukura, and H. Ohno, Physica E (Amsterdam) **6**, 817 (2000).
[8] A. Tackeuchi, O. Wada, and Y. Nishikawa, Appl. Phys. Lett. **70**, 1131 (1997).
[9] K. L. Litvinenko, B. N. Murdin, J. Allam, C. R. Pidgeon, M. Bird, K. Morris, W. Branford, S. K. Clowes, L. F. Cohen, T. Ashley, and L. Buckle, New J. Phys. **8**, 49 (2006).
[10] K. L. Litvinenko, L. Nikzad, J. Allam, B. N. Murdin, C. R. Pidgeon, J. J. Harris, T. Zhang, and L. F. Cohen, J. Appl. Phys. **101**, 083105 (2007).
[11] A. M. Gilbertson, M. Fearn, J. H. Jefferson, B. N. Murdin, P. D. Buckle, and L. F. Cohen, Phys. Rev. B **77**, 165335 (2008).
[12] W. Yang and Kai Chang, Phys. Rev. B **73**, 113303 (2006); W. Yang and Kai Chang, *ibid.* **74**, 193314 (2006).
[13] B. A. Bernevig, J. Orenstein, and S.-C. Zhang, Phys. Rev. Lett. **97**, 236601 (2006).
[14] Y. P. Varshni, Physica **34**, 149 (1967).
[15] N. S. Averkiev and L. E. Golub, Phys. Rev. B **60**, 15582 (1999); N. S. Averkiev, L. E. Golub, and M. Willander, J. Phys.: Condens. Matter **14**, R271 (2002).
[16] J. Kainz, U. Rössler, and R. Winkler, Phys. Rev. B **70**, 195322 (2004).
[17] W. Yang, K. Chang, and S. C. Zhang, Phys. Rev. Lett. **100**, 056602 (2008).
[18] J. Li, W. Yang, and K. Chang, Phys. Rev. B **80**, 035303 (2009).
[19] R. Winkler, *Spin-Orbit Coupling Effects in Two-Dimensinonal Electron and Hole Systems* (Springer-Verlag, Berlin, 2003), Chap. 7.
[20] I. Vurgaftman, J. R. Meyer, and L. R. Ram-Mohan, J. Appl. Phys. **89**, 5815 (2001).
[21] N. Dai, G. A. Khodaparast, F. Brown, R. E. Doezema, S. J. Chung, and M. B. Santos, Appl. Phys. Lett. **76**, 3905 (2000).
[22] E. O. Kane, in *Semiconductors and Semimetals*, edited by R. K. Willardson and A. C. Beer (Academic Press, New York, 1966), Vol. 1, p. 75.
[23] B. K. Ridley, *Quantum Processes in Semiconductors*, 2nd ed. (Oxford University Press, Oxford, 1988), Chap. 3.
[24] V. I. Puller, L. G. Mourokh, N. J. M. Horing, and A. Y. Smirnov, Phys. Rev. B **67**, 155309 (2003).